The FEBS Journal

FEBS PRESS science publishing by scientists

Lipids reverse supramolecular chirality and reduce toxicity of amyloid fibrils

Stanislav Rizevsky[1,2], Kiryl Zhaliazka[1], Mikhail Matveyenka[1], Kimberly Quinn[3] and Dmitry Kurouski[1,4]

1 Department of Biochemistry and Biophysics, Texas A&M University, College Station, TX, USA
2 Department of Biotechnology, Binh Duong University, Thu Dau Mot, Vietnam
3 BioTools, Inc., Jupiter, FL, USA
4 Department of Biomedical Engineering, Texas A&M University, College Station, TX, USA

Keywords
amyloid fibrils; insulin; lysozyme; supramolecular chirality; toxicity; VCD

Correspondence
D. Kurouski, Department of Biochemistry and Biophysics, Texas A&M University, College Station, TX 77843, USA
Tel: 1-979-458-3448
E-mail: dkurouski@tamu.edu

(Received 11 April 2022, revised 1 June 2022, accepted 22 June 2022)

doi:10.1111/febs.16564

Abrupt aggregation of misfolded proteins is a hallmark of many medical pathologies including diabetes type 2, Alzheimer and Parkinson diseases. This results in the formation of amyloid fibrils, protein aggregates with distinct supramolecular chirality. A growing body of evidence suggests that lipids can alter rates of protein aggregation. In this study, we investigated whether lipids could alter the supramolecular chirality of amyloid fibrils. We found that if present at the stage of protein aggregation, phospho- and sphingolipids uniquely reversed supramolecular chirality of insulin and lysozyme fibrils. Furthermore, amyloid fibrils with opposite supramolecular chirality exerted distinctly different cell toxicity. Specifically, insulin and lysozyme fibrils with reversed supramolecular chirality were less toxic to cells than the aggregates with normal supramolecular chirality. These findings point on the important role of lipids and supramolecular chirality of amyloid fibrils in the onset and progression of amyloid diseases.

Introduction

Diabetes type 2, Alzheimer and Parkinson diseases, as well as several other pathologies are associated with an abrupt deposition of misfolded proteins into various organs and tissues [1–3]. In these deposits, proteins are assembled into long fibrils that have cross-β-sheet secondary structure [4,5]. A growing body of evidence suggests that the structure and morphology of protein aggregates directly correlate with their toxicity [6–8]. Therefore, elucidation of physical, chemical, and biological factors that can alter the structure and morphology of fibrils is the focus of numerous biophysical studies reported over the past decade [8–11]. For instance, Kurouski et al. [12] reported that a small change in pH could alter the morphology and secondary structure of insulin fibrils. It has been found that aggregation of many other proteins including lysozyme, transthyretin fragment, and HET-S, a prion of the filamentous fungus *Podospora anserina*, can be controlled by pH [13]. Specifically, at pH below 2, these proteins aggregated forming tape-like fibrils, whereas at pH above this point, long-twisted fibrils were observed. In 2007, Ma et al. [14] reported that twists of fibrillar aggregates could be probed using vibrational circular dichroism (VCD). These fibrils exhibit a unique VCD spectrum with a negative peak at $\sim$ 1620 cm^{-1} and a set of positive peaks $\sim$ 1552, $\sim$ 1645, and $\sim$ 1665 cm^{-1}. Kurouski et al found that tape-like fibrils that form at pH below 2 exhibited almost a mirror-image VCD spectrum [12,15]. This observation suggested that these tape-like fibrils were composed of right-handed filaments. These results also demonstrated that VCD can be used to probe the

Abbreviations
CER, ceramide; CL, cardiolipin; Ins, insulin; LDH, lactate dehydrogenase; LUVs, large unilamellar vesicles; Lys, lysozyme; PS, phosphatidylserine; SM, sphingomyelin; VCD, vibrational circular dichroism.

macromolecular chirality of amyloid aggregates. This technique is based on photoelastic modulation of a linear infrared light in left- and right-circularly polarized states in the frequency range of tens of kilohertz [16]. After both left- and right-circularly polarized light pass through the sample of interest, their absorption is recorded using a mercury cadmium telluride (MCT) camera. The difference in absorption of left vs right circularly polarized light directly depends on the absolute chiral configuration and supramolecular organization of molecules present in the sample. Consequently, VCD can be used to determine the absolute chiral configuration of natural products and monitor chemical reactions, such as cyclobutane-1,2-d_2 thermolysis, which involve chiral compounds [17–20]. VCD is also capable of probing the supramolecular organization of biologically important macromolecules, such as proteins and DNA [21–24].

A growing body of evidence suggests that lipids play an important role in aggregation of misfolded proteins. For instance, Galvagnion et al. demonstrated that rates of aggregation of α-synuclein (α-Syn), a small cytosolic protein that is directly associated with Parkinson's disease, can be altered by lipids [25–27]. Dou et al. [5] showed that lipids not only alter the rates of α-Syn aggregation but also uniquely alter the secondary structure of protein oligomers. Similar findings were reported by Zhang et al. [28] for islet amyloid polypeptide protein (IAPP), which aggregation is linked to diabetes type 2. Specifically, the researchers showed that low levels of anionic lipids promoted IAPP aggregation and enhanced membrane permeabilization potential of these aggregates. At the same time, zwitterionic lipid did not alter the rate of IAPP aggregation, whereas cholesterol at or below physiological levels significantly decelerated IAPP amyloid formation, as well as lowered the propensity of IAPP aggregates to cause membrane leakage.

Expanding upon these fibrils, we investigated the extent to which lipids alter the morphology and supramolecular chirality of amyloid aggregates. For this, we aggregated insulin and lysozyme, proteins that are associated with injection amyloidosis and diabetes type 2, respectively, in the lipid-free environment and in the presence of lipids. We selected lipids that are commonly found in plasma and organelle membranes: phosphatidylserine (PS), ceramide (CER), sphingomyelin (SM), and cardiolipin (CL), a phospholipid that is primarily localized in the cytosolic side of mitochondrial membranes. All lipids except CER and SM were assembled into large unilamellar vesicles (LUVs) by a repeated procedure of freezing and thawing of the solutions of these lipids. These LUVs were ~ 100 nm in size, as was determined by dynamic light scattering. Next, insulin and lysozyme were mixed with the solutions of lipids in a 1 : 1 molar ratio and kept at 37 °C for 48 h under 510 rpm agitation (insulin) or at 65 °C for 7 days with no agitation (lysozyme).

Results and Discussion

Using atomic force microscopy, we examined the topography of insulin aggregates grown in the presence pf PS (Ins:PS), CL (Ins:CL), CER (Ins:CER), and SM (Ins:SM) as well as insulin fibrils grown in the lipid-free environment (ins), Fig. 1, A. We found that Ins: PS, Ins:CL, and Ins:SM samples contained short (30–60 nm) spherical aggregates and ~ 200 nm long fibrils that had 6–12 nm in height. Morphologically similar aggregates have been observed in Ins. However, Ins fibrils were significantly longer than Ins:PS, Ins:CL, Ins:CER, and Ins:SM aggregates, Fig. 1, A. Microscopic analysis of lysozyme aggregates grown in the presence of PS, CL, CER, and SM revealed predominance of thick (20–40 nm in height) fibrils, Fig. 1. We also observed that some of these fibrils were self-assembled into thicker bundles. In the lipid-free environment, aggregation of lysozyme yielded fibrils with similar morphologies and thicknesses (20–40 nm). However, these fibrils were much longer than Lys:PS, Lys:CL, Lys:SM, and Lys:CER aggregates. These findings show that lipids reduce the length of both insulin and lysozyme fibrils. These findings are in good agreement with the previously reported results by Terakawa et al. [29].

VCD is a unique tool that allows for elucidation of supramolecular organization of amyloid fibrils [30–32]. VCD analysis of insulin aggregates grown in the lipid-free environment, as well as in the presence of lipids revealed drastic differences between the spectra collected from these two groups of samples. Insulin fibrils grown in the lipid-free environment exhibited a 'normal' VCD spectrum, which was previously reported by several groups for insulin and lysozyme fibrils grown at pH above 2 [13,14]. This spectrum has a negative peak at ~ 1620 cm^{-1} and a set of positive peaks ~ 1645 and ~ 1665 cm^{-1}, Fig. 2, A. VCD spectra of Ins:CL, Ins:PS, Ins:SM, and Ins:CER were neatly mirrored images of the VCD spectrum collected from Ins sample. Specifically, these spectra had a positive band at ~ 1620 cm^{-1} and a set of negative bands at ~ 1645 and ~ 1665 cm^{-1}. These findings show that lipids reverse the supramolecular chirality of insulin fibrils in the protein aggregation is taken place in the presence of lipids.

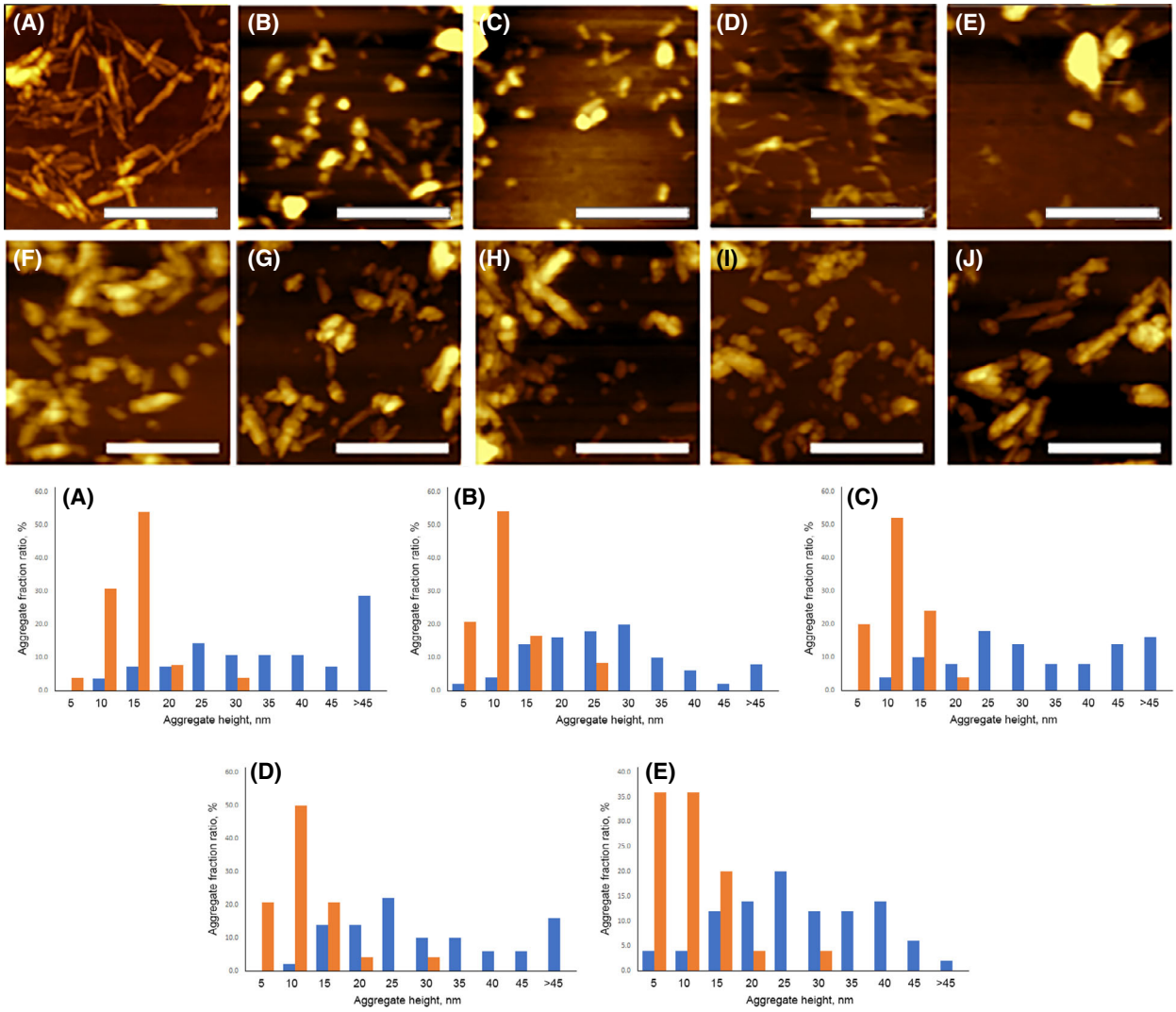

Fig. 1. Morphology of insulin and lysozyme aggregates grown in the lipid-free environment, as well as in the presence of lipids. AFM images (top) of ins (A), ins:CL (B), ins:SM (C), ins:PS (D), ins:CER (E) as well as Lys (F), Lys:PS (G) Lys:CL (H), Lys:SM (I), and Lys:CER (J). Insulin was aggregated with and without lipids at 37 °C under 510 rpm. Lysozyme aggregation was performed at 65 °C for 7 days without agitation. After that, sample aliquots were diluted with 1× PBS pH 3.0 and deposited onto pre-cleaned silicon wafer. AFM imaging was performed in tapping mode. Scale bars are 500 nm. Height profiles (bottom) protein aggregates of insulin (orange) and lysozyme (blue), grown without lipids (A) and in the presence of PS (B), CER (C), SM (D), and CL (E).

Although the position of the most-intense negative band ($\sim$1640 cm^{-1}) was the same for all Ins:CL, Ins:PS, Ins:SM, and Ins:CER, position of the second negative band varied for different samples, Fig. 2A. Specifically, it was found to be centered at 1665 cm^{-1} in the spectra collected form Ins:CL, Ins:CER, and Ins:SM, whereas in the spectra collected from Ins:PS, it was shifted to 1672 cm^{-1}. We also found that a positive band at $\sim$ 1620 cm^{-1} in the VCD spectrum of Ins:CL had a significantly lower intensity than the same band in the VCD spectra collected form Ins:CER, Ins:SM, and Ins:PS, Fig. 2A. These spectral changes point out on distinctly different supramolecular organization of Ins:PS and Ins:CL fibrils comparing with the supramolecular structure of Ins:CER and Ins:SM aggregates.

We found that amide I (1600–1700 cm^{-1}) and amide II (1500–1550 cm^{-1}) bands in the IR spectra collected from Ins, Ins:CL, Ins:PS, Ins:SM, and Ins:CER were very similar, Fig. 2B. The amide I band was centered at 1630 cm^{-1}, which demonstrates the dominance of parallel β-sheet in the structure of these aggregates [32]. We also observed a band at 1660 cm^{-1}, which points on the presence of unordered protein in the

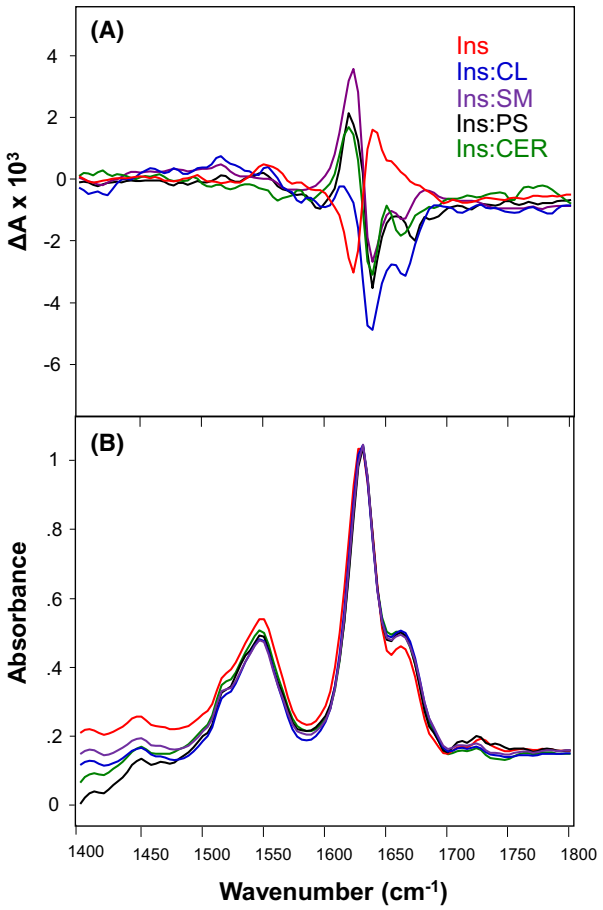

Fig. 2. Lipids reverse supramolecular chirality of insulin aggregates. VCD (top) and IR (bottom) spectra of ins, ins:CL, ins:SM, ins:PS, and ins:CER. VCD and IR spectra were acquired with 8 cm^{-1} resolution on DualPEM ChiralIR-2X Fourier transform VCD spectrometer.

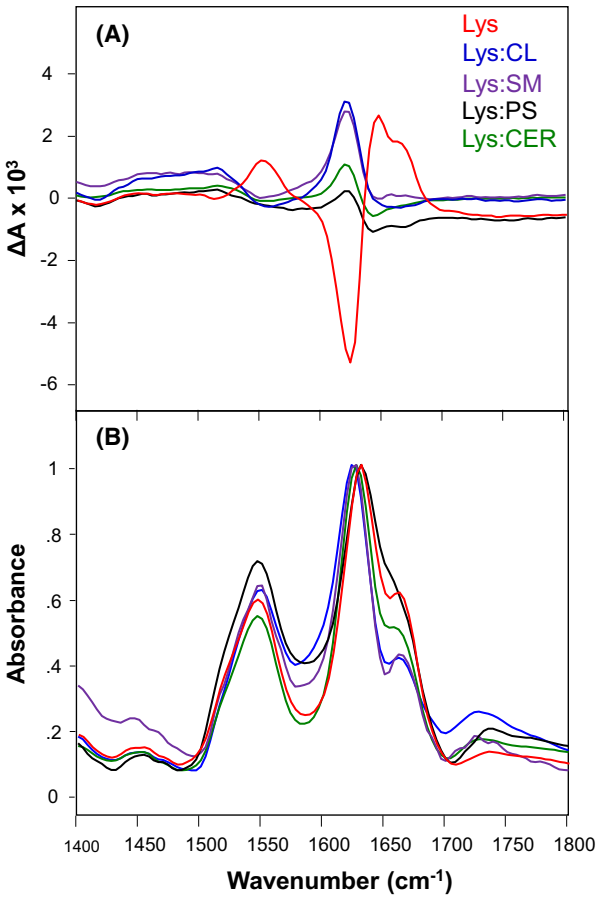

Fig. 3. Lipids reverse supramolecular chirality of lysozyme aggregates. VCD (top) and IR (bottom) spectra of Lys, Lys:CL, Lys:SM, Lys:PS, and Lys:CER. VCD and IR spectra were acquired with 8 cm^{-1} resolution on DualPEM ChiralIR-2X Fourier transform VCD spectrometer.

secondary structure of the analysed insulin aggregates [13]. Finally, we found a weak vibration around 1720 cm^{-1} in IR spectra collected from Ins:CL, Ins:PS, Ins:SM, and Ins:CER, Fig. 1B. This vibrational band can be assigned to the ester vibration of phospholipids [33]. This vibrational band indicate presence of lipids in the analysed samples of amyloid aggregates.

VCD spectra collected from lysozyme aggregates that were grown in the presence and absence of lipids also exhibit drastic differences, Fig. 3A. Lysozyme fibrils grown in the lipid-free environment exhibited, similar to insulin, the 'normal' VCD spectrum that had a negative peak at $\sim$ 1620 cm^{-1} and a set of positive peaks $\sim$ 1552, $\sim$ 1645, and $\sim$ 1665 cm^{-1} [13]. VCD spectra of Lys:PS, Lys:CL, Lys:SM, and Lys:CER exhibited the opposite intensity of the discussed above vibrations. Specifically, a positive band at $\sim$ 1620 cm^{-1} and a set of negative bands at $\sim$ 1552, $\sim$ 1645, and $\sim$ 1665 cm^{-1} was observed. These findings show that lipids also reversed the supramolecular chirality of lysozyme fibrils if present in the solution at the stage of protein aggregation.

Analysis of the IR spectra of lysozyme aggregates that were grown in the presence and absence of lipids revealed that Lys:CL, Lys:SM, and Lys:CER exhibited the band at 1626 cm^{-1} with the shoulder at 1663 cm^{-1}, Fig. 3B. This shows a predominance of parallel β-sheet with some contribution of unordered protein in the secondary structure of these aggregates. At the same time, we observed a shift of the amide I band to 1631 cm^{-1} in the IR spectra collected from Lys and Lys:PS. These shifts of amide I bands in the IR spectra, as well as discussed above VCD spectra point out on significant differences in the secondary structure of the analysed lysozyme aggregates that

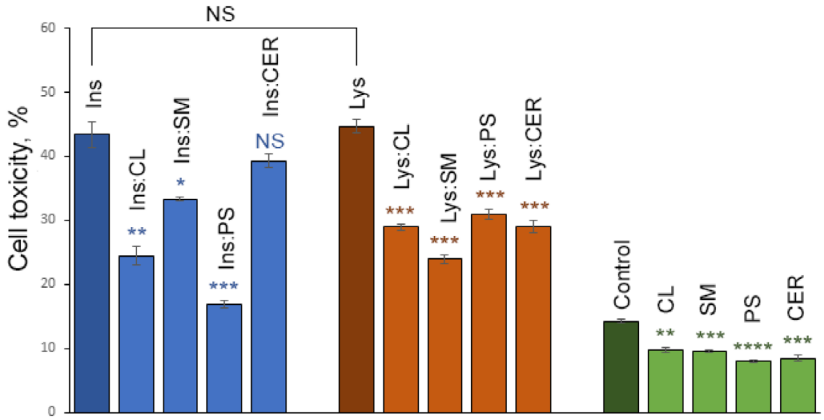

Fig. 4. Insulin and lysozyme aggregates grown in the presence of lipids are less toxic than the aggregates grown in the lipid-free environment. Histograms of LDH toxicity assays of ins, ins:CL, ins:PS, ins:SM, and ins:CER, as well as Lys, Lys:CL, Lys:SM, Lys:PS, Lys:CER aggregates. Toxicity of lipids themselves is shown in green. After 24 h of incubation of insulin (400 μM) with and without lipids at 37 °C under 510 rpm, sample triplicates were exposed to mice midbrain N27 cells for 48 h. for each of the presented results, three in-dependent measurements were made. Error bars represent standard errors of the mean (SEM) of three replicates. According to the *T*-test results, blue asterisks (*) show significance level of differences between ins and insulin aggregates grown in the presence of lipids. Brown asterisks show significance level of differences between Lys and lysozyme aggregates grown in the presence of lipids, whereas green asterisks show significance level of differences between lipids themselves and the control. NS is a nonsignificant difference, and $*P \leq 0.05$, $**P \leq 0.01$, $***P \leq 0.001$, and $****P \leq 0.0001$.

were grown in the presence of different lipids and lipid mixtures. Similar to the IR spectra collected from insulin fibrils that were grown in the presence of lipids, IR spectra of Lys:PS, Lys:CL, Lys:SM, and Lys:CER exhibit the vibrational band at 1720 cm^{-1}, which can be assigned to the ester vibration of phospholipids [33], Fig. 3, B. It should be noted that this band is absent in the IR spectra collected from lysozyme fibrils that were grown in the lipid-free environment. This observation points on the presence of lipids in the analysed samples of amyloid aggregates.

Next, we investigated the relationship between the supramolecular chirality of insulin and lysozyme fibrils and their toxicity. For this, we exposed mice midbrain N27 cell line to insulin and lysozyme aggregates grown in the presence and absence of lipids. After 24 h of incubation, cell viability was measured using lactate dehydrogenase (LDH) assay, Fig. 4.

LDH test indicated that Ins:CL, Ins:SM, and Ins:PS exhibited significantly lower cell toxicities compared with insulin aggregates grown in the lipid-free environment (Ins), Fig. 4. Specifically, toxicity of Ins:CL was twice, whereas toxicity of Ins:PS was more than three times lower than toxicity of Ins aggregates. Ins:CER exhibited similar cell toxicity to Ins aggregates. Similar results were observed for lysozyme fibrils. Specifically, we found that all lysozyme aggregates grown in the presence of lipids exerted significantly lower cell toxicity comparing to lysozyme fibrils grown in the lipid-free environment. Importantly, lipids themselves did not exert any significant cell toxicity.

Materials and methods

Materials

Bovine insulin and chicken egg white lysozyme were purchased from Sigma-Aldrich (St. Louis, MO, USA), 1,2-ditetradecanoyl-sn-glycero-3-phospho-L-serine (PS), 1′,3′-bis [1,2-distearoyl-sn-glycero-3-phospho]-glycerol [18 : 0 cardiolipin (CL)], sphingomyelin (SM), and ceramide (CER) were purchased from Avanti (Alabaster, AL, USA).

Liposome preparation

Large unilamellar vesicles (LUVs) of PS and CL were prepared accordingly to the method reported by Galvagnion et al. [34] Briefly, 0.6 mg of the lipid was dissolved in 2.6 mL of phosphate-buffered saline (PBS), pH 7.4. After the lipid was fully dissolved, the sample was heated to ~50 °C for 30 min in a water bath. Next, the vial was immersed in liquid nitrogen and kept there for 3–5 min. This thawing and freezing was repeated 10 times. After that, LUVs formation was finalized by passing lipid solutions through 100 nm membrane that was placed into the extruder (Avanti). LUV sizes were determined by dynamic light scattering. Due to the poor assembly properties, no LUVs for SM and CER were prepared; lipids used as received.

Insulin aggregation

After 400 μM of insulin was dissolved in PBS, pH was adjusted to pH 3.0 using concentrated HCl (Ins). For Ins:CL, Ins:CER, Ins:PS, and Ins:SM, 400 μM of insulin was mixed in equimolar concentration of the corresponding lipid. Next, the solution pH was adjusted to pH 3.0 using concentrated HCl. All samples were incubated at 37 °C under 510 rpm in the plate reader (Tecan, Männedorf, Switzerland) for 24 h.

Hen egg-white lysozyme aggregation

400 μM of hen egg-white lysozyme was dissolved in PBS; solution pH was adjusted to pH 3.0 using concentrated HCl (Lys). For Lys:CL, Lys:CER, Lys:PS, and Lys:SM, 400 μM of hen egg-white lysozyme was mixed with an equivalent concentration of the corresponding lipid; solution pH was adjusted to pH 3.0 using concentrated HCl. Next, the solutions were kept with no agitation in the block-heater (65 °C) for 7 days.

Vibrational circular dichroism (VCD)

VCD and Infrared (IR) spectra were measured at BioTools, Inc, Jupiter, FL using a dual-source, DualPEM ChiralIR-2X Fourier transform VCD spectrometer equipped with an MCT detector. The spectra were processed using GRAMS/AI 7.0 (Thermo Galactic, Salem, NH, USA).

AFM imaging

AFM analysis of the samples was performed using AIST-NT-HORIBA system (Edison, NJ, USA) equipped with silicon AFM probes (force constant 2.7 $N{\cdot}m^{-1}$ and resonance frequency 50–80 kHz). Scanning probes were purchased from Appnano (Mountain View, CA, USA). For each measurement, an aliquot of the sample was diluted with 1× PBS, pH 3.0, deposited onto pre-cleaned silicon wafer, deposited and dried under a flow of dry nitrogen. Analysis of collected images was performed using AIST-NT software. At least two independently prepared protein samples were measured by AFM to ensure full reproducibility of the reported results.

Cell toxicity assays

Mice midbrain N27 cells were grown in RPMI 1640 Medium (Thermo Fisher Scientific, Waltham, MA, USA) with 10% fetal bovine serum (FBS) (Invitrogen, Waltham, MA, USA) in 96 well-plate (5000 cells per well) at 37 °C under 5% CO_2. After 24 h, the cells were found to fully adhere to the wells reaching $\sim$ 70% confluency. N27 cells divide approximately once in 12 h. Consequently, after 24 h of cell incubation at 37 °C under 5% CO_2, each well contained approximately 10 000 cells. The cell count and viability were verified by Trypan Blue dye that confirmed the number of cell and their viability in the range of 98% to 99%. After that, 100 μL of the cell culture was replaced with 100 μL RPMI 1640 Medium with 5% FBS containing protein samples. This was done to lower the concentration of FBS which, in turn, was required by the LDH assay to lower the baseline absorbance level of the control. After 48 h of incubation, lactate dehydrogenase (LDH) assay was performed on the cell medium using CytoTox 96 non-radioactive cytotoxicity assay (G1781, Promega, Madison, WI, USA). Absorption measurements were made in plate reader (Tecan) at 490 nm. Every well was measured 25 times in different locations. At least two independently prepared protein samples were examined using LDH assay. All measurements were made in triplicates. *T*-test was used to determine significance level of differences between toxicity of analysed samples.

Conclusions

Our results show that lipids alter the supramolecular chirality of amyloid aggregates that are grown in their presence. Furthermore, changes in the secondary structure of protein aggregates formed in their presence directly depend on the chemical structure of the lipid. Acquired VCD spectra of insulin and lysozyme aggregates that were grown in the presence of major phosphor and sphingolipids present in cell and cell organelle membranes shows that these aggregates develop right-handed supramolecular chirality, whereas fibrils with the opposite handedness are formed from these proteins in the lipid-free environment. It should be also noted that this supramolecular chirality cannot be revealed using scanning probe microscopy. These findings are significant because the discussed above protein aggregates formed with and without lipids exert drastically different cell toxicity. Specifically, presence of lipids allows for substantial reduction of the toxicity exerted by such aggregates. Thus, cell toxicity of amyloid fibrils is likely to be determined by supramolecular chirality of the aggregates.

Acknowledgements

The authors are grateful to Biotools Inc. for providing access to the VCD instrument, as well as to Rina K. Dukor and Laurence A. Nafie for helpful discussions. We are grateful to the US National Institute of General Medical Sciences (R35GM142869) for the provided financial support.

Conflict of interest

The authors declare no conflict of interest.

Author contributions

SR planned experiments, performed experiments, and analysed data; KZ planned experiments, performed experiments, and analysed data; KQ planned experiments, performed experiments, and analysed data; MM planned experiments, performed experiments, and analysed data; DK conceptualized the work and wrote the paper.

Peer review

The peer review history for this article is available at https://publons.com/publon/10.1111/febs.16564.

Data availability statement

The data that support the findings of this study are available upon a request.

References

1 Chiti F, Dobson CM. Protein misfolding, amyloid formation, and human disease: a summary of Progress over the last decade. *Annu Rev Biochem*. 2017;**86**:27–68.
2 Knowles TP, Vendruscolo M, Dobson CM. The amyloid state and its association with protein misfolding diseases. *Nat Rev Mol Cell Biol*. 2014;**15**:384–96.
3 Iadanza MG, Jackson MP, Hewitt EW, Ranson NA, Radford SE. A new era for understanding amyloid structures and disease. *Nat Rev Mol Cell Biol*. 2018;**19**:755–73.
4 Chen SW, Drakulic S, Deas E, Ouberai M, Aprile FA, Arranz R, et al. Structural characterization of toxic oligomers that are kinetically trapped during alpha-synuclein fibril formation. *Proc Natl Acad Sci USA*. 2015;**112**:E1994–2003.
5 Dou T, Zhou L, Kurouski D. Unravelling the structural Organization of Individual alpha-synuclein oligomers grown in the presence of phospholipids. *J Phys Chem Lett*. 2021;**12**:4407–14.
6 Paravastu AK, Qahwash I, Leapman RD, Meredith SC, Tycko R. Seeded growth of beta-amyloid fibrils from Alzheimer's brain-derived fibrils produces a distinct fibril structure. *Proc Natl Acad Sci USA*. 2009;**106**:7443–8.
7 Kurouski D, Van Duyne RP, Lednev IK. Exploring the structure and formation mechanism of amyloid fibrils by Raman spectroscopy: a review. *Analyst*. 2015;**140**:4967–80.
8 Rizevsky S, Matveyenka M, Kurouski D. Nanoscale structural analysis of a lipid-driven aggregation of insulin. *J Phys Chem Lett*. 2022;**13**:2467–73.
9 Cataldi R, Chia S, Pisani K, Ruggeri FS, Xu CK, Šneideris T, et al. A dopamine metabolite stabilizes neurotoxic amyloid-beta oligomers. *Commun Biol*. 2021;**4**:19.
10 Vosough F, Barth A. Characterization of homogeneous and heterogeneous amyloid-beta42 oligomer preparations with biochemical methods and infrared spectroscopy reveals a correlation between infrared Spectrum and oligomer size. *ACS Chem Nerosci*. 2021;**12**:473–88.
11 Jinsmaa Y, Sullivan P, Sharabi Y, Goldstein DS. DOPAL is transmissible to and oligomerizes alpha-synuclein in human glial cells. *Auton Neurosci*. 2016;**194**:46–51.
12 Kurouski D, Lombardi RA, Dukor RK, Lednev IK, Nafie LA. Direct observation and pH control of reversed supramolecular chirality in insulin fibrils by vibrational circular dichroism. *Chem Commun (Camb)*. 2010;**46**:7154–6.
13 Kurouski D, Lu X, Popova L, Wan W, Shanmugasundaram M, Stubbs G, et al. Is supramolecular filament chirality the underlying cause of major morphology differences in amyloid fibrils? *J Am Chem Soc*. 2014;**136**:2302–12.
14 Ma S, Cao X, Mak M, Sadik A, Walkner C, Freedman TB, et al. Vibrational circular dichroism shows unusual sensitivity to protein fibril formation and development in solution. *J Am Chem Soc*. 2007;**129**:12364–5.
15 Kurouski D, Dukor RK, Lu X, Nafie LA, Lednev IK. Normal and reversed supramolecular chirality of insulin fibrils probed by vibrational circular dichroism at the protofilament level of fibril structure. *Biophys J*. 2012;**103**:522–31.
16 Nafie LA. Vibrational optical activity: principles and applications. Chichester, UK: Wiley; 2011.
17 Merten C, Berger CJ, McDonald R, Xu Y. Evidence of dihydrogen bonding of a chiral amine-borane complex in solution by VCD spectroscopy. *Angew Chem Int Ed Engl*. 2014;**53**:9940–3.
18 Chickos JS, Annamalai A, Keiderling TA. Thermolysis of (1R,2R)-1,2-dideuteriocyclobutane. An application of vibrational circular dichroism to kinetic analysis. *J Am Chem Soc*. 1986;**108**:4398–402.
19 Batista JM Jr, Blanch EW, Bolzani Vda S. Recent advances in the use of vibrational chiroptical spectroscopic methods for stereochemical characterization of natural products. *Nat Prod Rep*. 2015;**32**:1280–302.
20 Wang F, Wang Y, Polavarapu PL, Li T, Drabowicz J, Pietrusievicz MK, et al. Absolute configuration of tert-Butyl-1-(2-methylnaphthyl) phosphine oxide. *J Org Chem*. 2002;**67**:6539–41.
21 Wang L, Keiderling TA. Helical nature of poly(dI-dC).Poly(dI-dC). Vibrational circular dichroism results. *Nucl Acids Res*. 1993;**21**:4127–32.

22 Wang L, Yang L, Keiderling TA. Vibrational circular dichroism of A-, B-, and Z-form nucleic acids in the PO2-stretching region. *Biophys J*. 1994;**67**:2460–7.
23 Shanmugasundaram M, Kurouski D, Wan W, Stubbs G, Dukor RK, Nafie LA, et al. Rapid filament supramolecular chirality reversal of HET-s (218-289) prion fibrils driven by pH elevation. *J Phys Chem B*. 2015;**119**:8521–5.
24 Yasui SC, Keiderling TA. Vibrational circular dichroism of polypeptides. 8. Poly(lysine) conformations as a function of pH in aqueous solution. *J Am Chem Soc*. 1986;**108**:5576–81.
25 Alza NP, Iglesias Gonzalez PA, Conde MA, Uranga RM, Salvador GA. Lipids at the crossroad of alpha-synuclein function and dysfunction: biological and pathological implications. *Front Cell Neurosci*. 2019;**13**:175.
26 Galvagnion C. The role of lipids interacting with α-synuclein in the pathogenesis of Parkinson's disease. *J Parkinsons Dis*. 2017;**7**:433–50.
27 Galvagnion C, Brown JW, Ouberai MM, Flagmeier P, Vendruscolo M, Buell AK, et al. Chemical properties of lipids strongly affect the kinetics of the membrane-induced aggregation of alpha-synuclein. *Proc Natl Acad Sci USA*. 2016;**113**:7065–70.
28 Zhang X, St Clair JR, London E, Raleigh DP. Islet amyloid polypeptide membrane interactions: effects of membrane composition. *Biochemistry*. 2017;**56**:376–90.
29 Terakawa MS, Yagi H, Adachi M, Lee YH, Goto Y. Small liposomes accelerate the fibrillation of amyloid beta (1-40). *J Biol Chem*. 2015;**290**:815–26.
30 Measey TJ, Schweitzer-Stenner R. Vibrational circular dichroism as a probe of fibrillogenesis: the origin of the anomalous intensity enhancement of amyloid-like fibrils. *J Am Chem Soc*. 2011;**133**:1066–76.
31 Fulara A, Lakhani A, Wojcik S, Nieznanska H, Keiderling TA, Dzwolak W. Spiral superstructures of amyloid-like fibrils of polyglutamic acid: an infrared absorption and vibrational circular dichroism study. *J Phys Chem B*. 2011;**115**:11010–6.
32 Kurouski D. Advances of vibrational circular dichroism (VCD) in bioanalytical chemistry. A review. *Anal Chim Acta*. 2017;**990**:54–66.
33 Taniguchi T, Manai D, Shibata M, Itabashi Y, Monde K. Stereochemical analysis of glycerophospholipids by vibrational circular dichroism. *J Am Chem Soc*. 2015;**137**:12191–4.
34 Galvagnion C, Buell AK, Meisl G, Michaels TCT, Vendruscolo M, Knowles TPJ, et al. Lipid vesicles trigger α-synuclein aggregation by stimulating primary nucleation. *Nat Chem Biol*. 2015;**11**:229–34.